About Oligothiophene Self-Assembly: From Aggregation in Solution to Solid-State Nanostructures

Ph. Leclère,*,†,‡ M. Surin,† P. Viville,† R. Lazzaroni,† A. F. M. Kilbinger,§ O. Henze,§ W. J. Feast,§ M. Cavallini,|| F. Biscarini,|| A. P. H. J. Schenning,‡ and E. W. Meijer‡

Service de Chimie des Matériaux Nouveaux, Université de Mons-Hainaut/Materia Nova, Place du Parc, 20, B−7000 Mons, Belgium, Laboratory of Macromolecular and Organic Chemistry, Eindhoven University of Technology, PO Box 513, NL−5600 MB Eindhoven, The Netherlands, IRC in Polymer Science and Technology, Durham University, South Road, Durham DH1 3LE, United Kingdom, and Consiglio Nazionale delle Ricerche (CNR), Istituto per lo Studio dei Materiali Nanostrutturati (ISMN), Via P. Gobetti 101, I−40129 Bologna, Italy

Received March 1, 2004. Revised Manuscript Received July 14, 2004

Well-defined π-conjugated oligomers play an important role in the field of organic electronics, because their precise chemical structure and conjugation length give rise to well-defined functional properties and facilitate control over their supramolecular organization. In this review, we present different complementary approaches for the control of molecular assembly into well-defined structures on the nanoscale, applied to oligothiophenes as a typical conjugated system. We consider self-assembly in solution, sublimation of individual molecules in the vapor phase, and aggregation in thin deposits from compounds molecularly dispersed in a solution. We demonstrate that the development of substituted, soluble π-conjugated materials allows not only a control of their organization in the solid state but also the possibility of determining the degree of order in solution. During these self-assembly processes, the interplay between the conjugated molecules, the solvent, and the substrate surface is of primary importance. Depending on the interactions between the molecules and the substrate, one-dimensional (nanowires) or two-dimensional (platelets) objects can be generated. The self-organization of conjugated building blocks in solution or on surfaces, leading to the construction of nanoscopic and mesoscopic architectures, represents a starting point for the construction of molecular electronics or even circuits, through surface patterning with nanometer-sized objects.

1. Introduction

Nanoscopic and mesoscopic order in π-conjugated systems is a topic of utmost importance, because it determines the performance of the materials when used as components in organic electrooptical devices such as solar cells,[1] light-emitting diodes (LEDs),[2] and field-effect transistors (FETs).[3,4] Well-defined π-conjugated oligomers play an important role in this field, because their precise chemical structure and conjugation length gives rise to well-defined functional properties and facilitates control over their supramolecular organization.[5] Until recently research in this field has been focused mainly on methodologies for the synthesis and characterization of π-conjugated oligomers with long axis dimensions up to 10 nm.[6−8] Another major issue, which attracts increasing attention, is the control of the spatial orientation and packing of oligomers through the design of molecular and supramolecular architectures. The control of molecular assembly to give well-defined structures on the nanoscale can be carried out via different complementary approaches: (i) Self-assembly can take place in solution; the details of the aggregation behavior are governed by parameters such as the substitution on the conjugated backbone, the nature of the solvent, or the temperature. (ii) Because conjugated oligomers can be sublimed, it is also possible to follow their assembly as they form thin deposits on surfaces from individual molecules in the vapor phase; in that case, interactions with a solvent are absent and the driving forces controlling the aggregation are the intermolecular interactions between the conjugated species and the substrate surface. (iii) Another possibility is to generate thin deposits from conjugated compounds molecularly dispersed in a solution; aggregation takes place during the deposition and then depends on the interplay among the conjugated molecules, the solvent, and the substrate surface.

Oligomers and polymers based on α,α′-linked thiophenes are at the forefront of organic semiconductor materials with potential for applications in FETs and related structures.[9] To achieve easy processability of these materials, one common route is to substitute the thiophene backbone, either on the β-positions of the rings or on the two terminal α-positions. The corre-

* Corresponding author. Phone: + 32 65 37 38 68. Fax: + 32 65 37 38 61. E-mail: Philippe@averell.umh.ac.be.
† Université de Mons-Hainaut/Materia Nova.
‡ Eindhoven University of Technology.
§ Durham University.
|| Istituto per lo Studio dei Materiali Nanostrutturati (ISMN).

10.1021/cm049673x CCC: $27.50
Published on Web 08/24/2004

sponding substituted systems, generally bearing alkyl chains, are soluble, allowing the use of processing techniques such as spin-coating and solution casting for device fabrication.[10] For β-substituted polythiophenes, the search for soluble materials led to the concomitant development of strategies for the synthesis of regioregular polymers.[10a,11] The degree of regioregularity has been shown to influence crystallinity, conjugation, conformational order, and charge carrier properties. Similarly, the problem of solubility in oligothiophenes was overcome by the introduction of alkyl groups at the β-position or the terminal α-positions.[12] For sexithiophenes, it was demonstrated that the substitution pattern considerably influences the molecular packing and thereby the orientation in the crystal.[5,7,9] In particular, β-substitution leads to a distortion of the molecular conformation and to a larger intermolecular separation in the aggregated state, while α,α′-disubstituted sexithiophenes resemble the unmodified system in terms of close packing and degree of order.[13] Recently, other derivatives, such as branched[14] and star-shaped[15] oligothiophenes, have been synthesized and used for the fabrication of electronic devices.

In fact, the development of substituted, soluble π-conjugated materials allows not only a control of their organization in the solid state but also the possibility of determining the degree of order in solution. This has generated a great deal of interest in the supramolecular organization of such systems in organic solvents.[16] For example, studies of the organization in solution of chirally β-substituted polythiophenes provided profound insights into the solid-state organization of solution cast films.[17] The formation of supramolecular interactions via hydrogen-bonding arrays in combination with π−π stacking has also been used to self-assemble oligothiophenes into one-dimensional arrays on surfaces, generating a material with remarkable high charge carrier mobility.[18] In other examples, the Langmuir−Blodgett or the layer-by-layer technique[19] have been used for the self-assembly of monolayers of oligo- or polythiophenes.[20,21] Alternatively, the self-organization properties of various types of copolymers have been exploited by incorporating conjugated segments in macromolecules.[22] Another major advantage of the oligothiophenes in terms of processability is the fact that the compounds can be sublimed and condensed into thin films, under well-defined deposition conditions.

In fact, the self-organization of conjugated building blocks in solution or on surfaces, leading to the construction of nanoscopic and mesoscopic (10−1000 nm) architectures, can represent a starting point for the construction of molecular electronics[23] or even circuits,[24] through surface patterning with nanometer-sized objects.[25] In other words, these investigations constitute a step forward toward organic nanoelectronics.

In this context, the design of well-defined, easily processable thiophene oligomers, combined with a detailed understanding of their ordering arising from interactions in solution or in the solid-state, is needed to evolve sound protocols for the formation and manipulation of well-defined supramolecular structures, to improve the device performances.[26] As mentioned above, this work reviews three different approaches that we have used in the past few years to control the assembly of oligothiophene molecules. Our aim here is to collect the results that we have obtained with those three approaches and to point out how a set of experimental parameters (substitution pattern, solvent, temperature, deposition conditions) can be exploited to drive the molecular assembly toward well-defined nanostructures. The work described in this paper is therefore organized as follows: after the presentation of the structures of the oligothiophene series under study in section 1, section 2 describes the aggregation properties of the compounds in solution. For this study, UV−vis absorption and fluorescence spectroscopies, along with circular dichroism (CD) measurements in the case of chiral compounds, proved to be effective techniques for understanding aggregate formation. Section 3 is devoted to thin film formation from molecules in the vapor phase. To gain insight into the molecular assembly process, it is essential to collect morphological information on the very first stages of film formation, from the submonolayer regime to a few layer thickness. This is best achieved using scanning probe microscopy techniques, in particular atomic force microscopy (AFM). Section 4 deals with molecular assembly at surfaces, for deposits generated from solutions. This aspect of the study also uses AFM as the major morphology characterization tool for the deposited thin films. Finally, the morphological data are combined with the results of molecular simulations, to propose models for the solid-state assembly of the oligothiophene molecules.

The chemical structures of the oligothiophenes under study are shown in Figure 1. Besides unsubstituted sexithiophene **1**, which is the prototype compound for studies of vacuum-sublimed thin deposits, we have considered quinquethiophene, sexithiophene, and septithiophene molecules (5T, 6T, and 7T, respectively), end-capped at the α terminal positions by one or two short, flexible, and strongly hydrophilic segments of poly(ethylene oxide) (PEO). A few compounds with an alkyl chain are also considered. All these substituents provide solubility in common organic solvents such as tetrahydrofuran (THF), chloroform, or toluene. Note that the molecules of series **3** and **4** carry a methyl group on a carbon atom of the ethyleneoxide segment; such molecules are chiral, and stereocontrolled synthesis allows the production of *S*,*S*′ and *R*,*R*′ compounds, i.e., series **3** and **4**, respectively. As shown below, chiral molecules provide additional information on the assembly process. The synthesis of the α,α′-substituted compounds is described in refs 22a, 27, and 28; these series of molecules thus allow us to explore the correlation between the molecular structure, the aggregation behavior, and the microscopic morphologies.

2. Aggregation in Solution

The UV−vis absorption and fluorescence spectra recorded for **2a** in THF ($2.6\ 10^{-5}$ M) and *n*-butanol are presented in Figure 2a. The spectra obtained in THF are typical for molecularly dissolved α,α′-terminally disubstituted sexithiophene chromophores.[29] The fluorescence spectrum has a maximum at 528 nm (2.35 eV) and shows a characteristic vibronic fine structure, while the high intensity observed provides further evidence that the material is molecularly dissolved. Compound **3b**, which differs from **2a** by the two methyl groups on

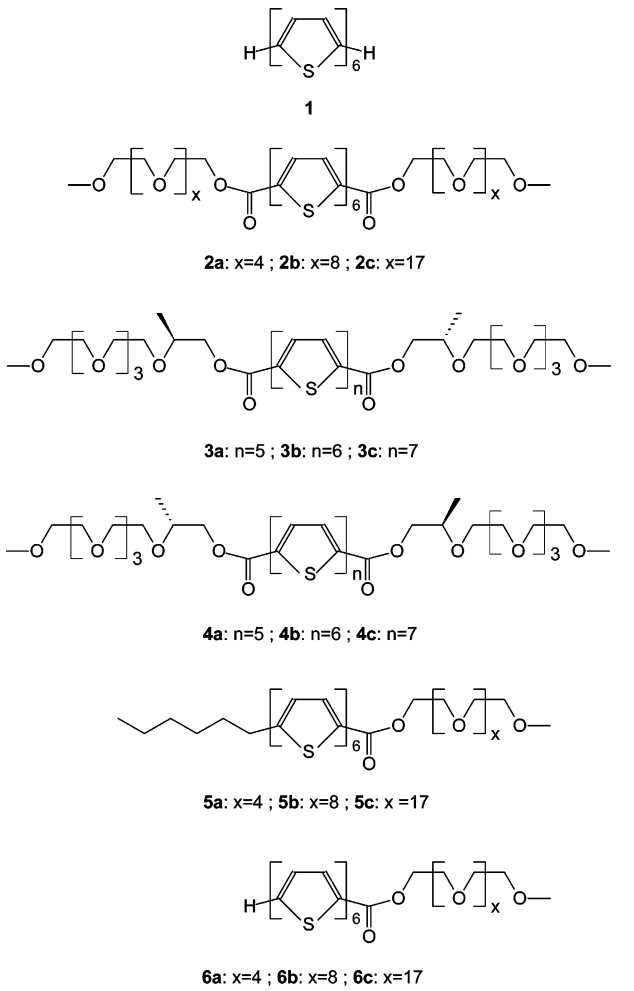

Figure 1. Chemical structure of the studied oligothiophenes.

the PEO segments, shows the same signature as **2a** in absorption and fluorescence; it is therefore also molecularly dispersed. The absence of aggregation is also confirmed by the absence of a CD signal for **3b** in this solvent.

In contrast, solutions of **3b** in *n*-butanol at 20 °C show a UV−vis absorption spectrum typical for aggregated sexithiophene derivatives[30] with a main band at λ_{max} = 403 nm (3.08 eV), blue-shifted by ca. $\Delta\lambda$ = 50 nm (ΔE = 0.34 eV) compared to a chloroform or THF solution, in which the compound is molecularly dissolved. In the case of solutions of **2a** in *n*-butanol, an even larger blue shift is observed, $\Delta\lambda$ = 71 nm (ΔE = 0.51 eV), λ_{max} = 381 nm (3.25 eV) (Figure 2a). The fluorescence intensity of solutions of both compounds in *n*-butanol is reduced when compared to THF solutions and the luminescence maximum is red-shifted. These observations, together with evidence of aggregation with increasing solvent polarity from nanospray FT-ICR mass spectrometry measurements,[31] strongly support the fact that these compounds aggregate in *n*-butanol while they are molecularly dissolved in THF. The shape and the size of these aggregates can be investigated by AFM measurements on deposits prepared from *n*-butanol solutions. The deposits of compound **3b** on a mica surface show a microscopic morphology of small rods lying on the substrate (Figure 2b); the average length and width of those aggregates (obtained from the analysis of 180 objects) is 100 ± 15 nm and 50 ± 15 nm, respectively. The height is about 7.0 ± 3 nm. These structures are likely to be related to the aggregates whose formation is deduced from solution spectroscopic studies. While the resolution in AFM is not sufficient to provide information on the internal structure of the aggregates, useful indications can be obtained from the CD spectra of the chiral systems.

A bisignate CD-effect is indeed observed for the *S*,*S*′ compound **3b** in *n*-butanol (Figure 3a); it exhibits a negative Cotton effect at low energy (λ = 400−700 nm) and a positive Cotton effect at higher energy (λ < 400 nm). The zero-crossing is within 5 nm of the absorption maximum of the chromophore, indicating strong exciton coupling in the sexithiophene aggregates.[32] Circular polarization of the fluorescence of **3b** in *n*-butanol is also observed. A maximum dissymmetry factor (g_{lum}) of −2.2 ± 0.2 10^{-3} at λ = 650 nm is found, for which the sign is in agreement with the sign of the CD at low energy.[33] Hence, well-defined chiral aggregates of **3b** are formed in *n*-butanol that not only possess a chiral ground state but a chiral excited state as well, indicating that the chirality is the result of supramolecular ordering. The larger blue shift in the UV−vis spectrum found for aggregates of **2a** in solution could indicate that these structures are better packed (due to the absence of the methyl branch on the PEO end group), resulting in a stronger exciton coupling.[34]

Compounds **3b** and **2a** also show aggregation in water at room temperature. Both UV−vis absorption spectra are quite similar to those of *n*-butanol solutions (main band at λ_{max} = 406 nm for **3b** and λ_{max} = 381 nm for **2a**). Again, the fluorescence maximum is red shifted (600 nm) with respect to that observed in THF solution and the intensity is reduced, indicating aggregation. A bisignate CD-effect is observed for **3b** in water, exhibiting a negative Cotton effect at lower energy and a positive Cotton effect at higher energy. Interestingly, when an apolar solvent like hexane is used, the same type of absorption spectrum is also found, indicating that the same type of aggregates are also formed in this solvent. Considered together, these data indicate that the variation between molecular dissolution and aggregation in solution is a subtle function of solvent polarity, with aggregation occurring both in nonpolar and strongly polar solvents and molecular dissolution prevailing in slightly polar solvents. The aggregation process is probably driven by oligothiophene−oligothiophene interactions and the inherent insolubility of unsubstituted oligothiophenes. From this hypothesis, we can propose that the aggregates have a core−shell morphology with the oligothiophene segments forming the core and the solubilizing shell consisting of a corona of PEO segments, the exact organization of the oligothiophene in the core being structure, solvent, and formation protocol dependent (vide infra).

The temperature dependence of the aggregation process in *n*-butanol solutions is studied in the range from −10 to 80 °C, using CD, UV−vis absorption, and fluorescence spectroscopy (parts a, b, and c of Figure 3, respectively). Initially solutions are cooled to −10 °C and then warmed to 70 °C slowly and stepwise with 10 min allowed for equilibration of the sample at each recording temperature. Below 20 °C, the UV−vis, CD, and fluorescence spectra of **3b** are typical of aggregated

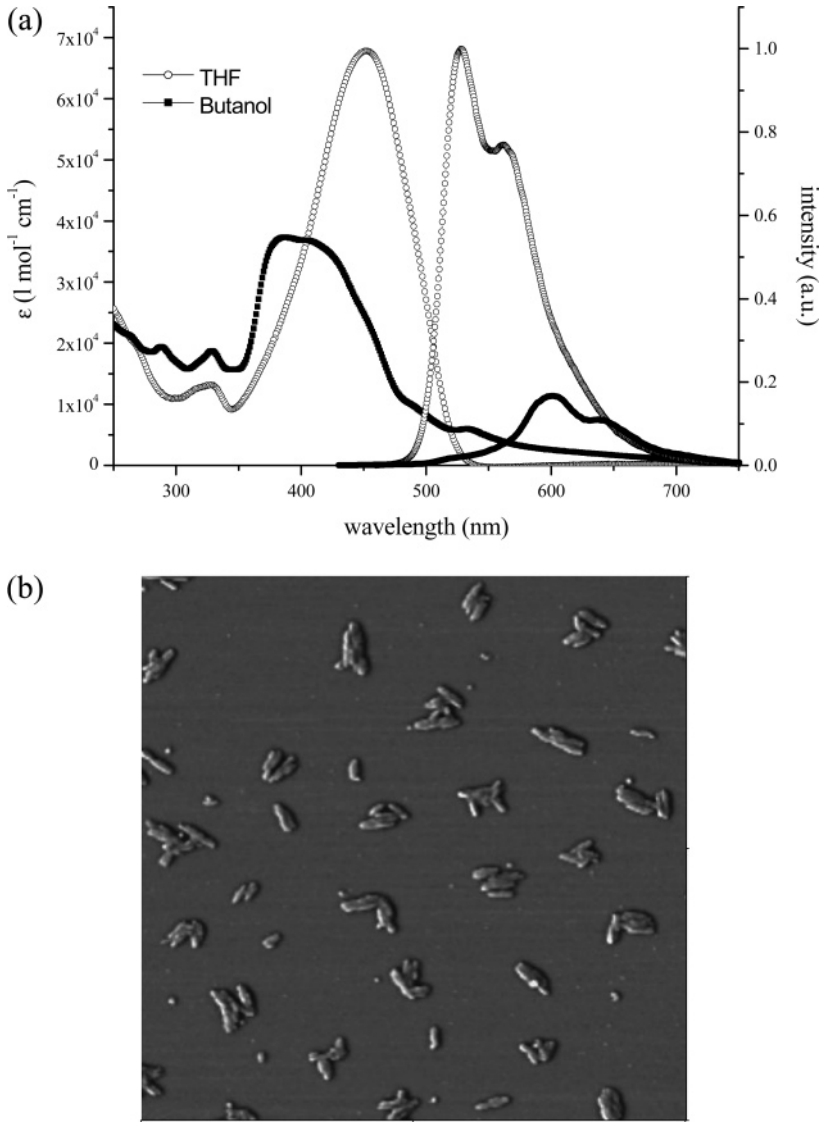

Figure 2. (a) UV−vis absorption and fluorescence spectra of **2a** in THF and *n*-butanol; (b) AFM phase image (1.0 × 1.0 μm^2) of **3b** aggregates prepared from *n*-butanol solution.

sexithiophenes, while above 40 °C the signature of the molecularly dissolved species is obtained. The phase transition is fully reversible, as a subsequent cooling run gives identical spectra.[35] For solutions of **2a** recorded at the same concentration, a thermochromic behavior similar to that observed for **3b** is found, but the "melting transition"[36] occurs at a higher temperature. Note also that the "melting temperature" was found to be concentration-dependent. For example, at a concentration of 2.6×10^{-6} M of **2a** in *n*-butanol, the temperature was $T_m = 9$ °C, while at a concentration of 6.0×10^{-5} M this value was $T_m = 33$ °C.

When the monomer/aggregate ratio taken from the spectral maxima is plotted against temperature, a sharp transition is observed (Figure 4). The sigmoidal curves obtained can be fitted with the Boltzmann equation,

$$\alpha = \frac{1}{1 + e^{(T - T_m)/\Delta T}}$$

in which α is the fraction of aggregated molecules, T_m is the "melting temperature" at which $\alpha = 0.5$, and ΔT relates to the width of the transition.[37] In the case of **3b** in butanol, using the same concentrations in the UV−vis, CD, and fluorescence experiments, similar melting temperatures are found [$T_m = 28.3$ °C (CD), $T_m = 28.1$ °C (UV−vis), $T_m = 28.8$ °C (fluorescence)]. As can be concluded from the fitted curve, aggregation occurs in a temperature range of approximately 20 °C, which points to a strongly cooperative process.[38] The three techniques thus prove the existence of two phases in *n*-butanol solution, i.e. aggregates at low temperature and molecularly dissolved species at high temperature. These combined results unambiguously show that chiral aggregates are breaking up or are formed directly without an intermediate disordered aggregated state (in contrast to what has been observed previously for phenylene−ethynylene oligomers[39] and C_3-symmetrical disk-shaped molecules[38]). In the case of **2a**, a higher "melting temperature" in *n*-butanol is found ($T_m = 48.3$ °C). This difference is probably due to the absence of the methyl branch in the oligo(ethylene oxide) end groups of **2a**, resulting in a better packing and stronger aggregation, already seen in UV−vis data, which is more blue-shifted.

It is interesting to note that CD measurements of **3b** in water show a melting transition at $T_m = 34$ °C, while

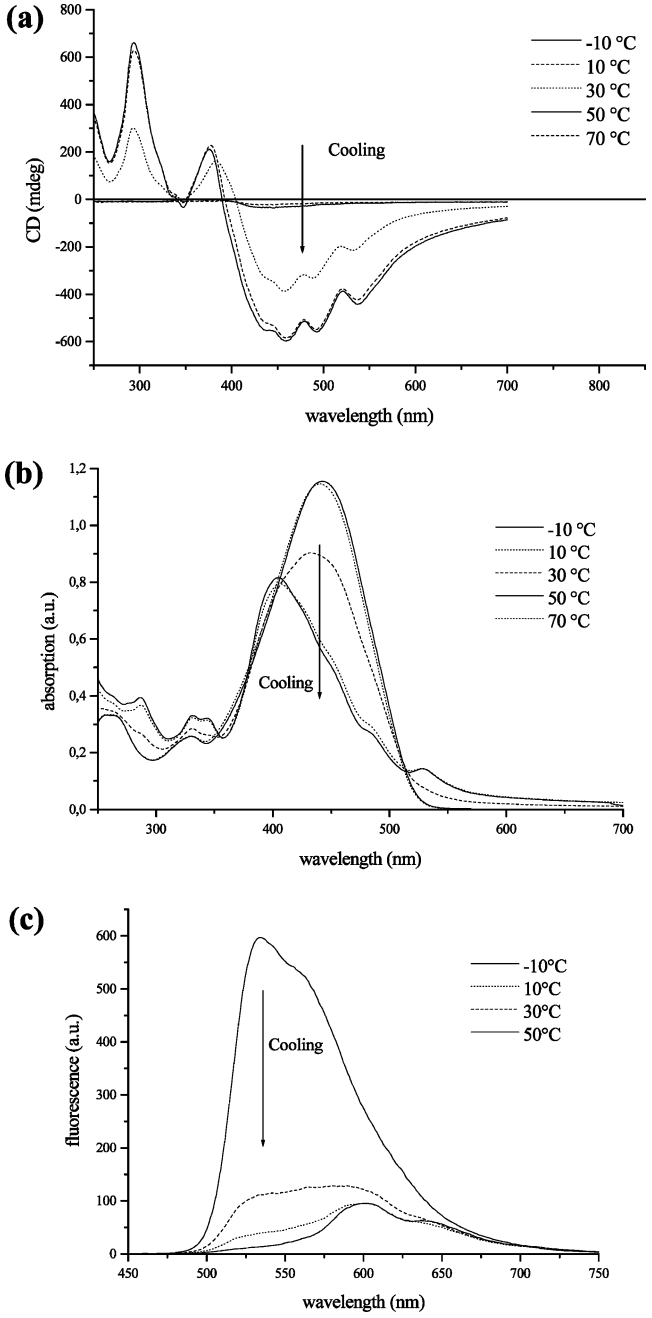

Figure 3. Temperature-dependent CD (a), UV−vis absorption (b), and fluorescence (c) spectra of **3b** in *n*-butanol (2.6×10^{-5} mol.l^{-1}).

UV−vis and fluorescence spectra do not show any transition. This is consistent with a transition from chiral helical aggregates to achiral disordered aggregates in which the end groups are more mobile and can no longer induce chiral information in the sexithiophene stack.

The UV−vis absorption spectrum of septithiophene compounds (**3c**, **4c**) in THF shows a structureless band at $\lambda_{max} = 452$ nm (2.74 eV). Surprisingly, this absorption is similar to that found for the sexithiophene analogue, suggesting that saturation in conjugation length already occurs in the hexamer. This is in contrast with the observations made by Bauërle et al. suggesting that a gradual red-shift occurs up to the dodecamer (12T).[40] The absorption spectrum in *n*-butanol at 70 °C (Figure 5) has a shape similar to that observed in tetrahydrofuran, and the absorption maximum is located at almost the same position ($\lambda_{max} = 454$ nm, 2.73 eV). Upon cooling to 20 °C, this main band shifts to the blue by ca. $\Delta\lambda = 41$ nm ($\Delta E = 0.27$ eV) to $\lambda_{max} = 413$ nm (3.00 eV). Since the same blue shift was found for sexithiophene assemblies (vide supra), we are led to the conclusion that aggregation of the 7T chromophores also occurs in *n*-butanol.

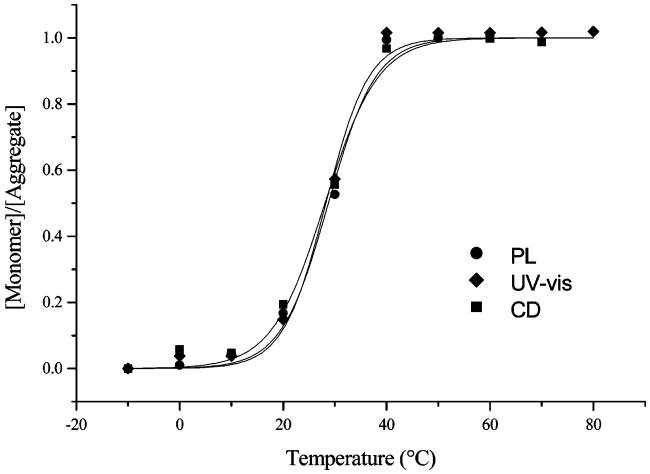

Figure 4. Monomer/aggregate ratio versus temperature for **3b** in *n*-butanol (2.6×10^{-5} mol L^{-1}) and the fitted curves.

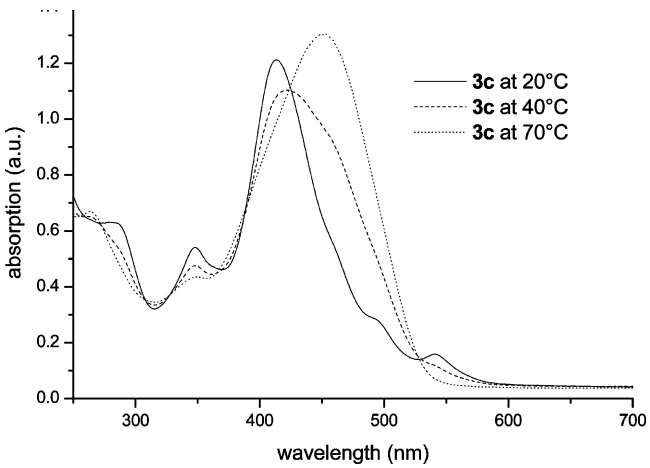

Figure 5. UV−vis spectra of **3c** in *n*-butanol at different temperatures.

The melting temperature of the assemblies depends also on the conjugation length of the oligothiophene block. When the variable temperature measurements in *n*-butanol are performed with comparable concentrations of **3a** (5T), **3b** (6T), and **3c** (7T), the melting transition temperature for the stacks rises with conjugation length as a result of more favorable $\pi-\pi$ interactions. Compound **3a** is molecularly dissolved in *n*-butanol, even at 0 °C while **3b** has a melting transition at 28.4 ± 0.4 °C and **3c** melting temperature of around 50 °C. This phase transition is fully reversible.

Chirality in aggregates can arise from the presence of only a small proportion of chiral molecules in an assembly of largely achiral molecules; this phenomenon is generally known as the "sergeant and soldiers" effect.[41] Chiral **3b** was tested as the potential "sergeant" to direct the packing of the "soldiers", i.e., achiral **2a**. However, mixing a small amount of **3b** in *n*-butanol solutions of **2a** does not result in amplification of the

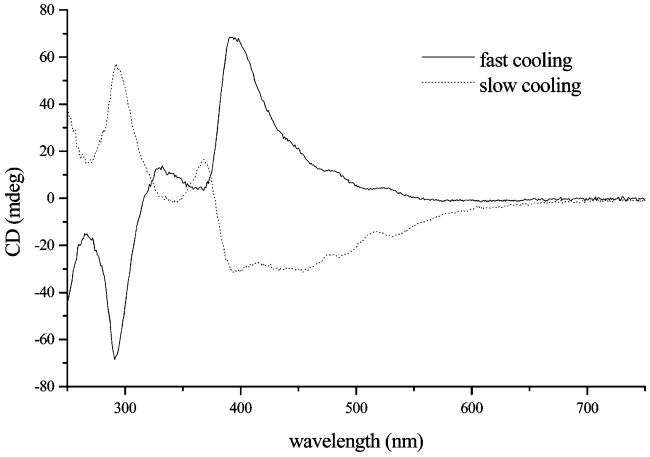

Figure 6. Cotton effect observed after fast and slow cooling of a 1:3 mixed solution of **3b** and **2a**.

CD effect. A linear relation is observed between the mole fraction of **3b** and the CD effect, indicating that there is no exchange between the aggregates of **2a** and **3b** under these conditions. Amplification of the chirality is found only when the solutions are heated above the aggregate "melting temperature" and then slowly cooled (Figure 6). After addition of 30 mol % of "sergeant" molecules, all stacks have gained the same chirality as stacks exclusively formed from "sergeant" **3b**. Although the percentage of "sergeants" used is relatively high, this result illustrates that the "sergeant and soldiers" phenomenon operates in *n*-butanol.[42] However, the rate of cooling is crucial: when mixtures of **3b** and **2a** in 1:3 molecular ratio are cooled slowly, a CD spectrum similar to that obtained from pure **3b** is found, but fast cooling produces a CD spectrum that is the inverse of that obtained by slow cooling (Figure 6). This phenomenon has been observed previously for low-molecular weight organic compounds and polymers in the solid state.[43] Slow cooling gives the thermodynamically most stable form of the mixed aggregate, while fast cooling gives the kinetically favored form. It is interesting to note that the "melting temperature" of aggregates of **2a** is higher than that for aggregates of **3b**, which suggests that aggregates of **2a** act as seeds for the aggregating mixtures. Further work is needed to gain a detailed understanding of the remarkable phenomena of mixed ordered aggregate formation.

3. Oligothiophene Assembly from the Vapor Phase

In the growth of thin deposits by high-vacuum sublimation, a flux of hot gas molecules impinges onto a colder substrate surface so that condensation takes place before the thermal equilibration of the molecules is achieved. The resulting morphology depends on (i) the intrinsic molecular properties, (ii) the nature of the substrate−molecule interactions, and (iii) the kinetics of growth (e.g., impinging rate, nucleation, diffusion, coalescence, reorganization, desorption). The latter is controlled by the interplay among experimental parameters, such as the deposition rate, the temperature of the substrate, and the amount of deposited material.

Therefore, it is important to understand and control the kinetics of growth in order to infer the basic relations between film structure, molecular assembly, and the relevant electrical and optical properties. Here we describe the vacuum deposition approach for the controlled formation of thin films of unsubstituted sexithiophene **1** (6T). Oligomers are the most appropriate compounds for such a study, because they can be sublimed without chemical degradation. It was found by X-ray diffraction (XRD) that films of **1** grown at room deposition temperature possess long-range molecular order,[44−46] indicating that there is a spontaneous tendency toward ordered aggregation. Upon increasing the deposition temperature, enhanced anisotropy in the electrical properties was observed, which correlates with structural and morphological changes observed by XRD and SEM, respectively.[47] These observations led to the hypothesis that films of compound **1** consist of stacked layers of 6T molecules with a more or less enhanced molecular order within each layer. Preliminary evidence that layered growth in oligothiophenes on silicon substrate starts from the early stages of the process was obtained from AFM observations on quinquethiophene (5T),[48] albeit an extensive investigation at larger thickness was not carried out. It was shown by optical linear dichroism[49] that the ordered growth of **1** decreases and eventually fades out at increasing thickness. Furthermore, the dominant growth direction, i.e., whether the molecular orientation with respect to the substrate is planar or perpendicular, depends on the nature and structure of the substrate.[50] Thus, it is important to carry out growth studies with well-defined and well-characterized surfaces, for instance, atomically smooth and clean surfaces such as mica, highly oriented pyrolitic graphite. Mica offers the advantage that its hydrophilic surface might be a reasonable model for the growth on the technologically more relevant silicon wafers, ITO, and glass. Here we describe the formation of thin deposits of molecule **1** on freshly cleaved mica, aimed at elucidating the molecular assembly aspects as well as the basic kinetics of film growth.

The morphology of 6T thin films is very sensitive to the growth conditions.[51−54] A broad morphological diversity, ranging from islands to layers and lamellae can be obtained upon a variation of experimental parameters. Such complexity arises from the dominance or suppression of one or more intervening mechanism of growth as the diffusion of molecules on the forming film is changed by the deposition temperature, the amount of material, and the time of growth.

The early stages of growth involve nucleation and formation of islands. Density of nuclei, lateral size, height, and molecular order within the islands depend on the deposition temperature. At room temperature the islands (from a few hundred nanometers to micrometers in diameter) exhibit regular features (Figure 7a) and multiple peaks in the distribution of the topographical height which are integer multiples of 2.4 nm, i.e., the length along the long axis of **1**.[54] This indicates that the oligomer forms well-defined monomolecular layers, in which the molecules stand upright, perpendicular to the substrate (Figure 7c). Monomolecular terraces are also observed in deposits grown at 150 °C (Figure 7b); however, the islands are much larger (a few micrometers) and their edges are branched rather than regular, as in the growth of diffusion-limited aggregates.[55]

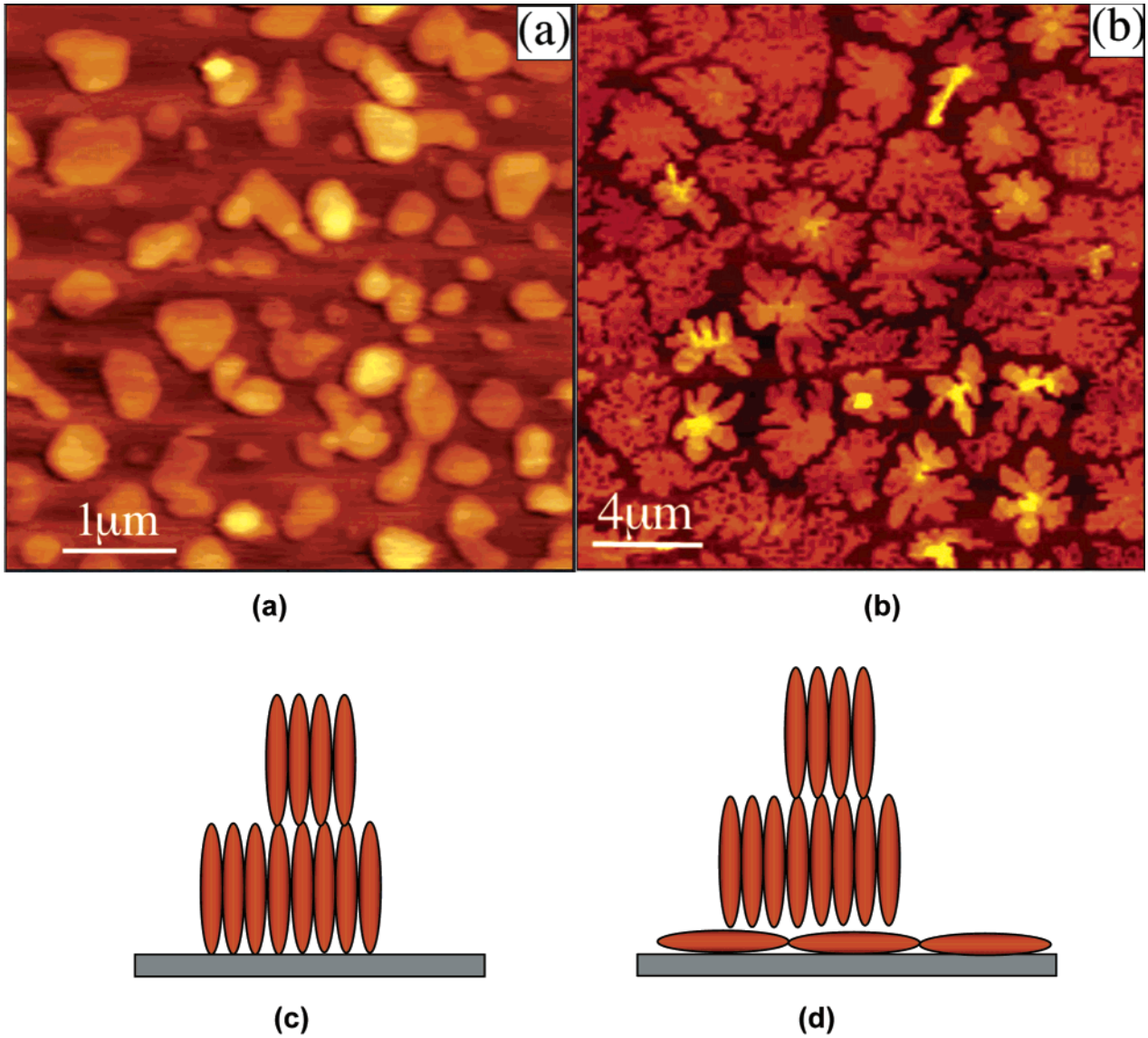

Figure 7. AFM images of 6T island growth at (a) deposition $T = 25$ °C, $h = 5$ nm; (b) $T = 150$ °C, $h = 3$ nm; (c and d) proposed model for the molecular organization for parts a and b, respectively.

With increasing thickness, the film morphology at room temperature becomes granular. Small grains (a few tens of nanometers in diameter) form upon completion of the film cover; thereafter, the morphology remains granular, with the grain size increasing with the amount of material deposited. The transition from 2D islands to 3D grains is reminiscent of a Stranski–Krastanov[55] growth transition, although owing to the nonequilibrium conditions, here this simple scheme should not strictly hold. It is interesting to compare the evolution of organization with thickness described above with that of a film grown at high temperature (150 °C) and depicted in Figure 8, where images were recorded on films 1, 3, 5, and 20 nm thick (parts a, b, c, and d, respectively). At 150 °C, nucleation of protrusions that are a few tens of nanometers wide takes place after almost complete coverage by the first monolayer has been achieved. This first monolayer exhibits a considerable degree of order as is apparent from the sharp edges around the voids. The average height of this monolayer with respect to the substrate is 0.6 nm, which suggests that molecules in this first layer lie edge-on, parallel to the mica surface. Around the outgrowths protruding from the first monolayer, the islands grow, and after their coalescence, the growth proceeds layer-by-layer (Figure 7d). The terrace height 2.3 ± 0.4 nm corresponds to the length of molecule **1**, i.e., the molecules in the film are oriented perpendicularly with respect to the surface. At about 50 nm thickness, proliferation of elongated nuclei occurs, which then leads to a network of oriented lamellae (Figure 8d) that might be simply the result of a change in the direction of growth. Such types of growth transitions might be specific to anisotropic compounds (such as elongated conjugated molecules) and cannot be strictly according to the canonical growth modes (Frank-van der Merwe, Stranski–Krastanov, Volmer–Weber) of atomistic growth processes.[55]

We have shown that, for a given thickness and increasing deposition temperature, the film morphology changes gradually, from grains to lamellae. This behavior is reminiscent of order–disorder phase transitions of the second order, although here the more ordered "phase" is obtained at higher temperature.[53] A convenient way to locate the transition is to observe the

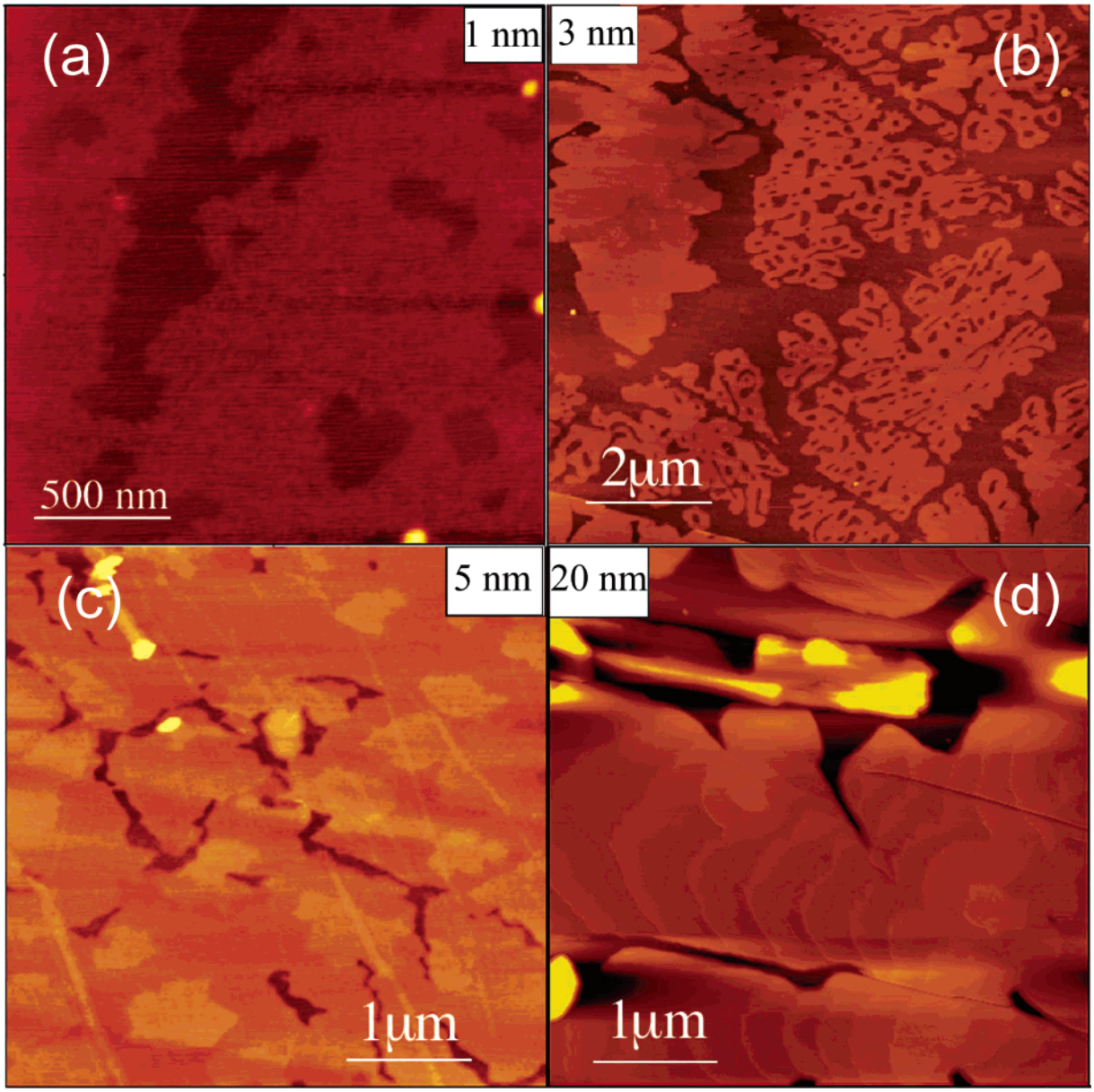

Figure 8. Evolution of the morphology with increasing amount of deposited material from a to d (reported as the nominal film thickness) at deposition $T = 150$ °C.

evolution of the orientational order of the domains (cos 2α, in Figure 9), and the details of the method are given in ref 52. With this approach, it is possible to determine a priori the different morphologies of films of **1** as a function of deposition temperature and thickness, as is illustrated in Figure 9 for the effect of temperature. The same type of analysis also shows that the transition from grains to lamellae with temperature occurs at lower temperature as the film thickness is decreased. Therefore, granular 6T films can be obtained at low deposition temperatures (a few tens of degrees Celsius), via a suitable decrease of thickness. This evidence is consistent with the evolution of molecular order monitored by optical dichroism.[56]

The evolution of shape and anisotropy in 6T films suggests that there is a progressive, rather than abrupt, increase in the molecular ordering and hierarchy of morphological structures as the deposition temperature increases. At higher temperatures and longer settle times (deriving from an interplay of deposition rate and film thickness), the molecules in the film have the possibility to find more stable forms of aggregation, which progressively approach the crystal phase. Therefore, by controlling the rate and the deposition temperature for a given thickness, it is possible to map a continuous set of metastable phases between the isotropic, disordered polycrystalline film up to the crystal. This is an important step toward a real control of the spatial arrangement of these molecules in a film, and the implications for controlling the optical and electrical properties are obviously relevant.

4. Oligothiophene Assembly from the Solution

From the thermodynamic stand point, assembly in solution (or the lack thereof) is governed by the interaction balance between the conjugated molecules and the solvent molecules, while the morphology of the deposits obtained by vacuum sublimation depends also on the molecule-surface interactions (with no involvement of the solvent). When generating thin solid-state deposits

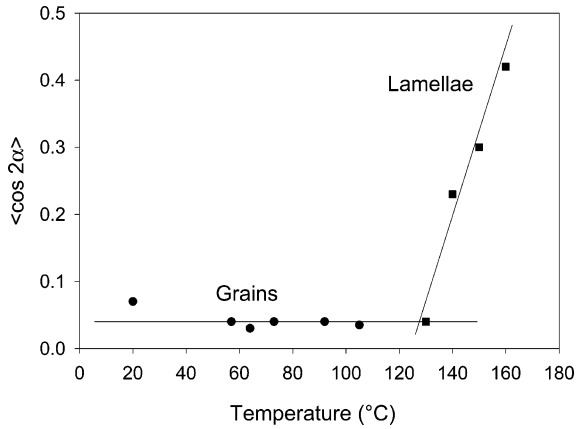

Figure 9. Orientational order parameter vs deposition temperature. Circles and squares are grains and lamellae, respectively. Straight lines represent the best fit for the lamellae data and mean value of the grain data, respectively.

from conjugated compounds molecularly dispersed in solution, upon slow evaporation, all three types of interactions (molecule−molecule, molecule−solvent, molecule−surface) are at play, which provides additional tenability for the controlled formation of conjugated nanostructures.

a. Molecular Organization into Monolayers. Using very dilute solutions allows the generation of deposits with a thickness in the range from one monolayer to a few layers. The morphology of the deposits on mica, as determined using AFM, can then be compared to the results obtained for the vacuum-deposited films. For all the molecules of series **2**−**6** (Figure 1), the microscopic morphology of deposits on mica from THF or toluene solutions (two solvents in which no aggregation takes place) exhibits ultrathin regular layers lying on the substrate, i.e., islands with a very regular height of few nanometers, with lateral dimensions varying from a few hundred nanometers to a few micrometers. An illustration of this type of structure is shown in Figure 10a for molecule **3b**. The regularity in the thickness of the layers is illustrated by a cross section of the height image (Figure 10b). In this case, the thickness is 2.7 ± 0.1 nm. The height of the islands is independent of the conditions of preparation (concentration, type of solvent) but depends only on the compound studied. Layers are sometimes stacked, as illustrated in parts c and e of Figure 10, which correspond to deposits of compounds **5c** and **5a**, respectively. In Figure 10c, the brightest spots correspond to a second layer on top of the first one; each layer being 7.1 ± 0.1 nm high. Layer stacking is even clearer in Figure 10e. The height histogram of that image (shown in Figure 10f) displays well-defined peaks, corresponding to individual layers. The period d between peaks provides a mean value for the layer thickness of 4.7 ± 0.1 nm. The predominance of large islands or "stepped pyramids" is not fully controlled; it probably depends on the interplay between the solvent dewetting and its evaporation. The important point, however, is that the layer thickness depends only on the chemical structure of the compound. To correlate the thickness values with the molecular architecture, molecular modeling is used to estimate the length of the various molecules in their fully extended configuration. The oligothiophene backbones are optimized with adjacent monomers in the S-anti configuration; the oligoethylene oxide (EO) and hexyl groups are considered in the all-trans configuration. The angle between the thiophene oligomer and the end groups is optimized, which can lead to a nonlinear shape (i.e., molecules with a bend between the oligothiophene and the end groups). In all cases, the length of the fully extended molecule is given as the distance between the extremities of the molecule. The thickness of the first layer is plotted vs the length of the fully extended molecules in Figure 11. We observe that (i) the thickness of the layers globally increases with the length of the molecule, and (ii) its value is always lower than the length of the fully extended molecules (the solid line represents the 1:1 ratio). That means that the molecules are not fully extended perpendicular to the substrate. Comparing sets of molecules differing by a single structural parameter can provide further information on the molecular orientation within the monolayers:

(1) In the symmetric molecules **3a**, **3b**, and **3c** (and **4a**, **4b**, and **4c**), the number of thiophene units is 5, 6, and 7, respectively, and the length of ethylene oxide groups is constant. The mean heights of the first layer in that series are respectively 2.2, 2.7, and 3.1 nm (±0.1 nm in each case), respectively. The estimated total length of the molecules is about 6.2, 6.6, and 7.0 nm, with the length of the conjugated segments being close to 2.0, 2.4, and 2.8 nm, for **3a**, **3b**, and **3c**, respectively. It is therefore clear that the molecules do not stand fully extended and perpendicular to the substrate. Notice, however, that the increase in the thickness when going from 5T- to 6T- to 7T-containing molecules (0.4−0.5 nm) is very close to the length of one thiophene unit (about 0.4 nm). That suggests that the conjugated segment is indeed perpendicular to the substrate plane. A (quasi-) perpendicular orientation is also observed for nonsubstituted oligomers (as described in section 3) and for other α,α′-substituted oligothiophenes deposited onto various substrates.[9] The fact that in the series the thickness of the layers is only slightly larger than the length of the conjugated segment suggests that one PEO group of each molecule lies flat on the substrate (this is probably favored by the ionic character of the mica surface), while the other one is strongly tilted relative to the substrate normal.

(2) When comparing sexithiophene systems symmetrically substituted with PEO segments of increasing length (compounds **2a**, **2b**, **2c**), one observes a steady increase in the layer thickness (marked with the broken line in Figure 11). Clearly, the conformation with the PEO groups flat on the surface and very strongly tilted vs the surface normal, which is proposed above for the compounds with the shortest PEO group (**3b** and **2a**), does not hold for their counterpart with longer PEO groups. Most probably, the tilt angle of those groups relative to the surface normal becomes lower as their length increases.

(3) The conformation of the hexyl groups can be inferred from the comparison of the compounds of series **5** and **6**. In compound **5a**, the length of the fully extended molecule is 5.1 nm, and the mean thickness of the layers is 4.7 ± 0.1 nm. For compound **6a** the layers are 4.0 ± 0.1 nm thick, with the length of the

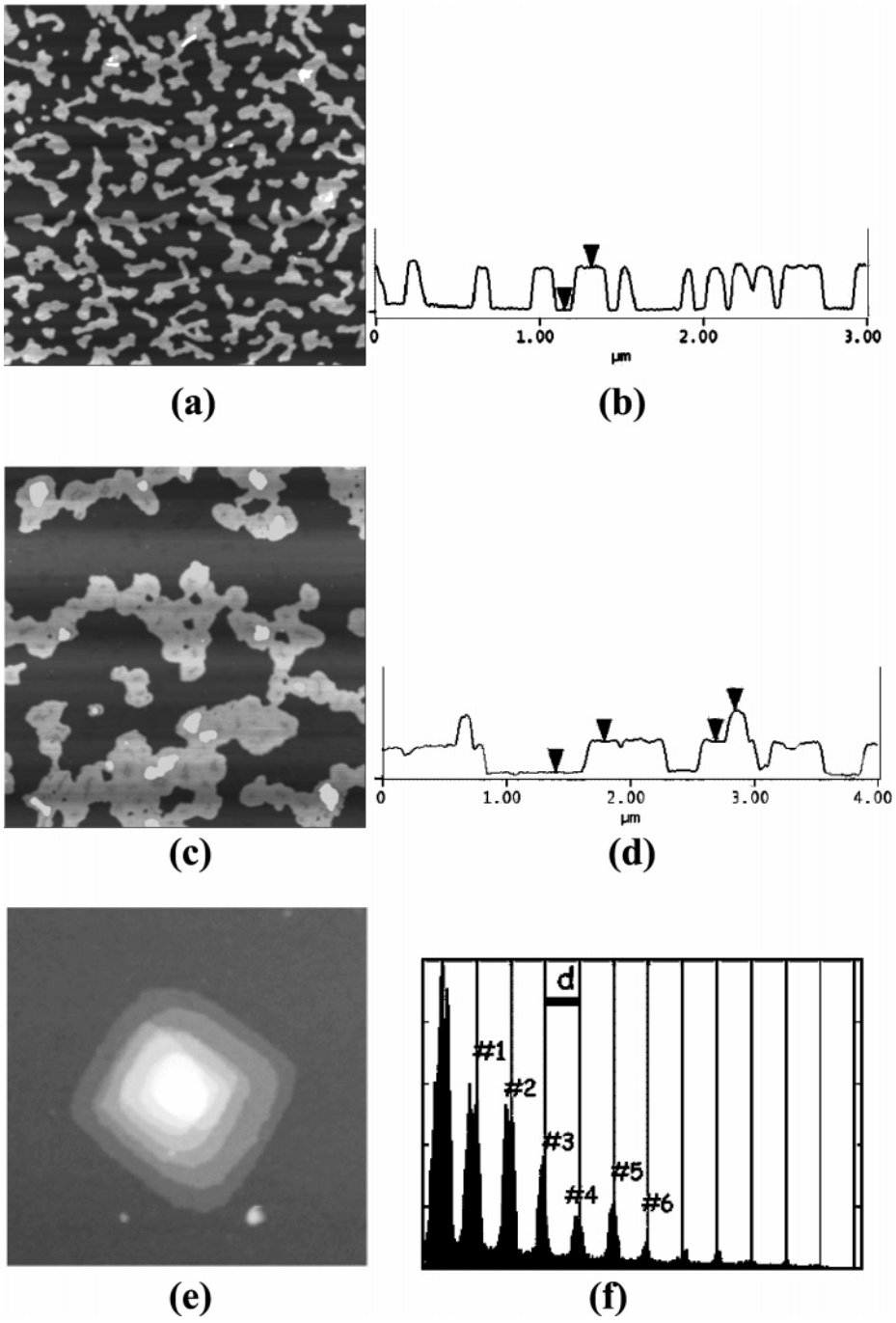

Figure 10. AFM height images of thin deposits (solution-cast) from THF on mica: (a) **3b** ($3.0 \times 3.0 \mu m^2$); (b) cross-section, height between cursors = 2.7 nm; (c) **5c** ($4.0 \times 4.0\ \mu m^2$); (d) cross-section, height between cursors = 7.1 nm; (e) **5a** ($2.0 \times 2.0\ \mu m^2$); (f) height histogram (d = 4.7 nm).

fully extended molecule being about 4.5 nm. Therefore, those two molecules stand nearly perpendicular to the substrate. The 0.7 nm increase in thickness of the layers from **6a** to **5a** is very close to the length of the hexyl group (8 Å), indicating that the hexyl end group is almost perpendicular to the substrate. This is confirmed by the comparisons between molecules **5b** and **6b** and between molecules **5c** and **6c**: in each case, an increase in layer thickness between 0.6 and 0.8 ± 0.1 nm is observed.

(4) Monosubstituted sexithiophene molecules seem to assemble very differently than disubstituted ones: compound **2a** (and **3b** and **4b**), with two $(EO)_5$ end groups, forms layers 2.7 ± 0.1 nm thick, whereas compound **6a**, with only one $(EO)_5$ end group, shows layers 4.0 ± 0.1 nm thick. The model of packing of the molecules of series **5** and **6** is therefore a quasiperpendicular orientation of the full molecules on the substrate, with no strong tilt of the PEO groups.

Globally, these results indicate that (i) the conjugated segments tend to orient perpendicular to the substrate plane, (ii) nonpolar substituents, e.g., hexyl groups, also orient perpendicular to the substrate. (Such orientation is consistent with the fact that the alkyl groups and the conjugated segments, being nonpolar, do not have a strong tendency to interact with the polar mica surface.), and (iii) the behavior of the PEO groups is more complex. The shortest PEO segments appear to be able

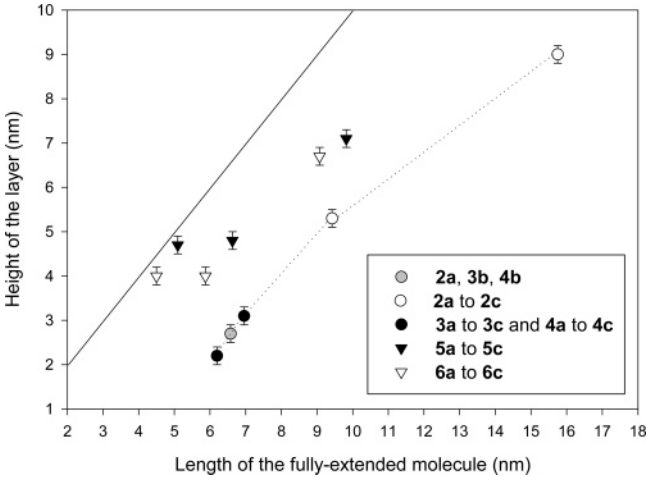

Figure 11. Comparison between the thickness of the first layer on mica (as measured with AFM) and the length of the molecules in their fully extended conformation (as calculated with molecular modeling). The gray dot actually belongs to three different series (**2**, **3**, and **4**).

to interact with the mica surface, whereas the orientation of longer segments is different.

Even though the structural information obtained from the AFM data on the very first monolayers is quite qualitative, it is nevertheless important because the transport processes in organic FET's take place in a very thin region (a few nanometers) in contact with the dielectric.[59,9b] Information on the molecular orientation within that region is therefore essential for the understanding of the device performances.

The perpendicular orientation of the conjugated backbone observed in the deposits formed from solution is identical to that of the sexithiophene molecules in the vacuum-sublimed films, indicating that the same driving force for assembly, i.e., $\pi-\pi$ interactions, is at work in both cases. It is noteworthy that the deposits formed from solution on mica never show a first layer for which the thickness would be consistent with the conjugated backbone parallel to the substrate, as is observed for the first layer of sublimed films made of molecule **1** generated at high temperature. Deposition from solution therefore corresponds to the low-temperature regime of vacuum deposition, for which the molecules in all layers are perpendicular to the substrate.

Nevertheless, for the compounds with two PEO substituents, the thickness of the first layer is systematically smaller (by 1 nm or more) than that of the overlayers. This is consistent with the presence of strong interactions between the PEO groups and the mica, which would increase the contact area between those groups and the surface, hence reducing the thickness of the first layer. The orientation of the oligothiophene segment is not modified, since an increase of 0.4 nm in thickness is also found when going from 5T- to 6T- to 7T-containing compounds.

b. Influence of the Substrate. To explore further the influence of the substrate on the supramolecular organization, thin deposits were generated onto graphite, which is an apolar surface. For symmetric molecules (series **2**, **3**, and **4**), straight fibrils are formed; this is illustrated in Figure 12, corresponding to deposits of compound **3b** on graphite. Figure 12a shows bundle of fibrils, while Figure 12b clearly shows isolated single

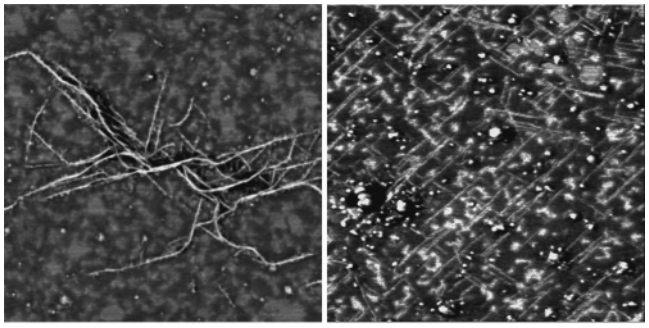

Figure 12. AFM phase images ($3.0 \times 3.0\ \mu m^2$) of thin deposits of **3b** on graphite substrate.

fibrils. The single fibrils are straight, from a few hundred nanometers to micrometers long, typically about 1 nm high, and their width correlates well with the computed length of the fully extended molecule (the measured width is 7 ± 1 nm and the length of the fully extended molecule is 6.6 nm). This suggests that the thin fibrils are one-molecule-wide π-stacks. The width of the large fibrils, such as those observed in Figure 12a, is a multiple of the length of the molecule in its fully extended configuration. They therefore correspond to the lateral aggregation of a few thin fibrils.

Molecular mechanics and dynamics simulations have been used to understand the packing of the molecules into these fibrillar structures, in terms of the orientation arising from specific interactions. The simulations have been realized with the universal force field (UFF),[57] which correctly describes the geometry and torsional behavior both for conjugated oligothiophenes and for saturated chains such as PEO. Simulations of one-dimensional stacks of **2a** have been carried out for clusters of two to 10 chains, with the conjugated segments in a cofacial arrangement. The results of the simulation on a 10 molecule stack are shown in Figure 13, where the oligothiophenes are shown with their short axis perpendicular to the view. The 6T segments remain planar, parallel to each other, at a typical interchain distance of 3.7−3.9 Å, which is in full agreement with the interchain distance determined in π-stacks of substituted polythiophene.[11c] We also observe a half-thiophene-unit lateral shift of the 6T segments relative to the two nearest neighbors.

From the AFM data in combination with the molecular modeling simulations, we can therefore propose that the fibrillar structures are made of a conjugated core of parallel π-stacked oligothiophenes (interchain distance 3.7−3.9 Å) with ethylene oxide groups on each side of the fibrillar axis. Therefore, conjugated chains are perpendicular to the fibril axis, edge-on over the substrate. The length of the ribbons indicates that such π-stacking can extend over micrometers, i.e., thousands of molecules. This type of 1D assembly is radically different from the morphology observed for the same compounds on mica.

It is interesting to note that the ribbons tend to be aligned along three directions at an angle of 120° to each other (Figure 12a). This arrangement is reminiscent of the 3-fold symmetry of the graphite surface, indicating that interactions with the substrate also play an important role in the chain assembly.

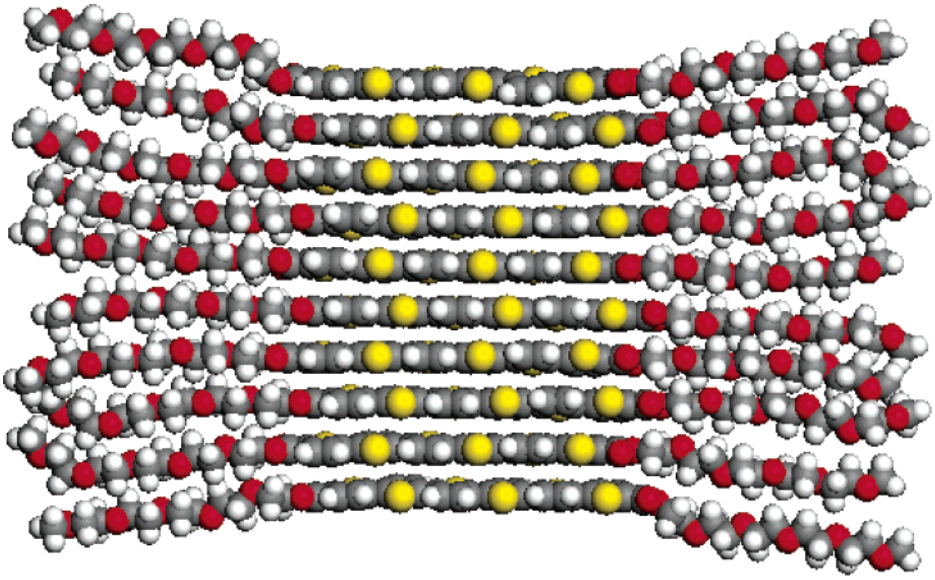

Figure 13. Optimized 10-chain cluster of **2a**, with the 6T short axis perpendicular to the view (sulfur atoms in yellow and oxygen atoms in red).

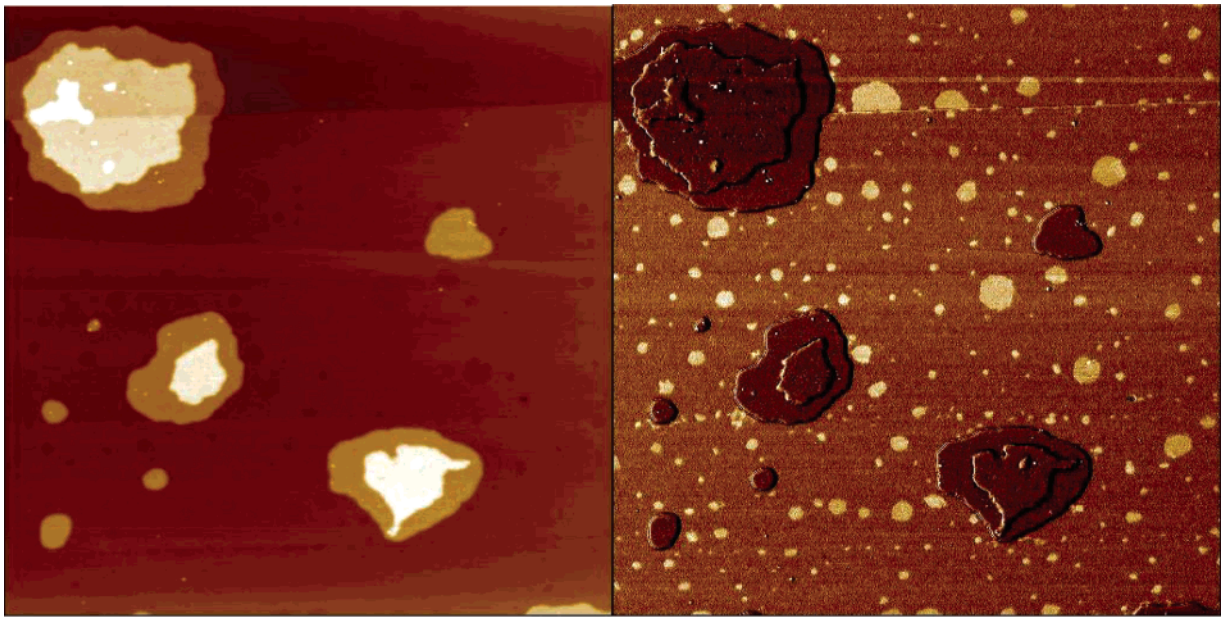

Figure 14. AFM height (a) and phase (b) images (2.5 × 2.5 μm^2) of a thin deposit of **6c** on graphite.

Changing the substitution pattern dramatically modifies the morphology: the asymmetrically substituted compounds of series **5** and **6** (which possess either only one PEO group or one PEO group and one hexyl group) do not form fibrillar assemblies on graphite. Instead, flat islands are observed; this is illustrated in Figure 14 for compound **6c**. Interestingly, the stacked layers forming the islands, with thicknesses of a few nanometers, appear to grow over a much thinner, quasicontinuous layer that is only about 0.3 nm thick. The presence of that layer is better visualized in the phase image, in which small areas of uncovered graphite surface appear with the brightest contrast. The thin layer corresponds to the light brown background and all the stacked layers in the islands appear with the same dark brown contrast. Since the phase contrast in tapping mode AFM can be interpreted in terms of the tip−sample interactions, Figure 14b clearly demonstrates that the thin layer has a different response compared to the graphite substrate and the islands.

The major morphological difference observed between the deposits made from symmetrical di-PEO-substituted compounds (fibrils) and those made from asymmetrically substituted molecules (layers) may be rationalized in the following way: conjugated systems have a strong tendency to lie flat on graphite, to favor $\pi-\pi$ interactions. Such a geometry is possible when a single PEO group is present. Alkyl chains also tend to lie flat on graphite; the presence of the hexyl groups must therefore also favor the flat conformation. In the presence of PEO groups on both sides of the conjugated system, intermolecular interactions between those groups prob-

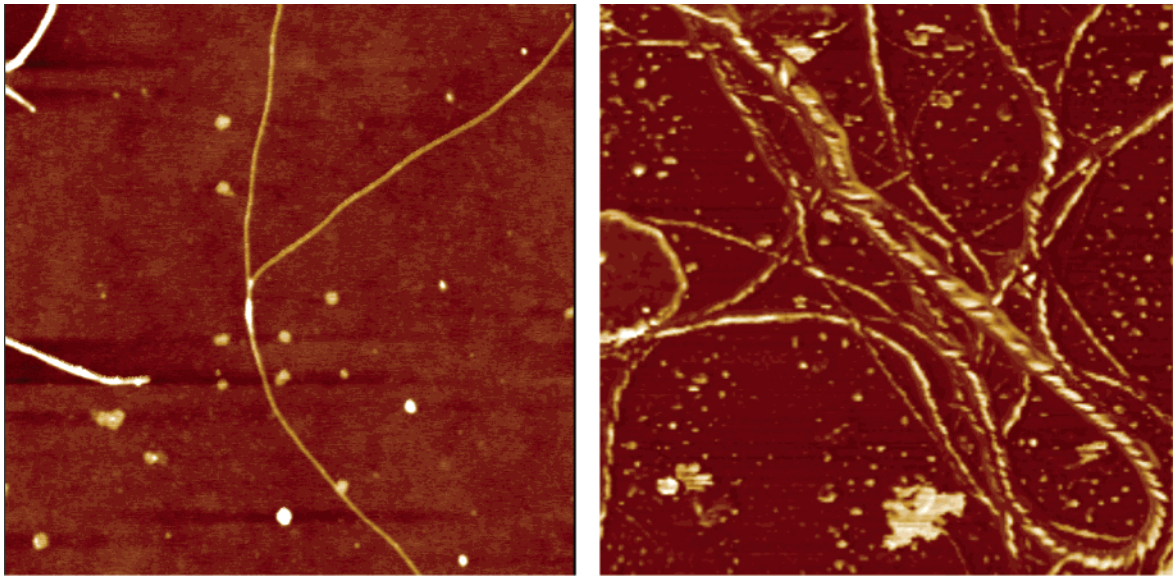

Figure 15. AFM images on silicon oxide of (a) **2b** ($5.0 \times 5.0\ \mu m^2$) and (b) **3b** ($2.5 \times 2.5\ \mu m^2$). Only **3b** shows left-handed helical aggregates.

ably prevent the oligothiophene segment from lying flat on the substrate. The edge-on geometry then becomes the most stable situation (it still allows for sizable interaction with the graphite surface), and $\pi-\pi$ stacking of conjugated units can therefore take place to generate fibrils.

In terms of surface polarity, the naturally oxidized surface of silicon is probably intermediate between strongly polar, ionic mica and apolar graphite.[58] The strong interactions involving the PEO substituents (with mica) on one hand and the conjugated units (with graphite) on the other hand might therefore not play such a strong role in defining the morphology of the deposits formed on silicon. Indeed, symmetric compounds with short PEO groups are found to organize into fibrillar assemblies (instead of islands or flat monolayers). Interestingly, while achiral compounds (such as **2a**) form flat featureless fibrils (Figure 15a), the assemblies built from their chiral counterpart (here compound **3b**) all appear as left-handed helical objects (Figure 15b). Clearly, the presence of a stereocenter in the molecule induces the formation of chiral assemblies in the solid state.[59] It is intriguing that the compound with inverted chirality (**4b**) assembles into fibrils that are also left-handed. This suggests that the formation of those chiral objects is not only due to the chiral nature of the building blocks, but also to some other (surface) effect that has to be understood.

Conclusions

Considering that the control of molecular assembly into well-defined structures on the nanoscale is a key parameter for the improvement of electronic nanodevices, we reviewed in this paper three different complementary approaches that we have used in the past couple of years for the fine-tuning the supramolecular organization of oligothiophenes. Those compounds are at the forefront of organic semiconductor materials with potential for applications in FETs and related structures. The study of the self-assembly of oligothiophenes having oligo(ethyleneoxide) tails that takes place in solution provides important information on the aggregation behavior. From our results, it appears that the self-assembly process is governed by the substitution on the conjugated backbone, the nature of the solvent, and the temperature. In particular, the collected data indicate that the evolution between molecular dissolution and aggregation in solution is a subtle function of solvent polarity, with aggregation occurring in nonpolar and strongly polar solvents and molecular dissolution prevailing in slightly polar solvents. The large blue shift in the UV−vis spectrum found for the aggregates indicates that these structures are tightly packed, resulting in a strong exciton coupling, which is also the case for vacuum-deposited films. Moreover, circular dichroism measurements show that when the molecules possess a chiral center in the oligoethylene oxide end groups, a Cotton effect is observed, indicating that the aggregates are chiral and that this chirality is the result of supramolecular ordering. Experiments performed by varying the temperature in *n*-butanol solutions prove the existence of a sharp transition temperature, increasing with the number of thiophene rings, between aggregates (at low temperature) and molecularly dissolved species (at high temperature). These combined results unambiguously show that chiral aggregates are breaking up or are formed directly without an intermediate disordered aggregated state. Those aggregates have a core−shell morphology with the oligothiophene segments forming the core and the solubilizing shell consisting of a corona of PEO segments, the exact organization of the oligothiophene in the core being structure, solvent, and formation protocol dependent. These conclusions can be extended to other solvents such as aqueous media, which constitutes an important issue for the development of biosensors.

Because the actual devices are in the solid state, it is also important to characterize the organization of

molecules within the aggregates in the solid state. These aggregates can be either obtained from deposits of oligothiophene solutions or from sublimation of oligothiophene molecules. In the later case, interactions with a solvent are absent and the driving forces controlling the aggregation are the intermolecular interactions between the conjugated species and with the substrate surface. Depending on the sample preparation conditions, the morphology (observed by AFM) of thin films made of 6T can be varied from islands to monolayers, lamellae, or granular deposits. The third possibility to generate organized nanostructures is from conjugated compounds molecularly dispersed in a solution. The aggregation by self-assembly takes place during the deposition and then depends on the interplay between the conjugated molecules, the solvent, and the substrate surface. Two-dimensional architectures can be obtained when the molecules are deposited on a strongly polar substrate such as mica, while one-dimensional objects (nanowires) are observed on graphite and silicon, indicating that the polarity of the substrate plays a major role in the assembly process. Preliminary results obtained on organic field-effect transistors with the active semiconducting layer made of a few monolayers of the studied compounds were recently reported.[60] It is possible in that case to establish a clear and direct correlation between the transistor performance (carrier mobilities of $10^{-2}-10^{-3}$ cm^2/V s and the on/off current ratio of 10^3-10^5) and the morphology within the ultrathin layer.

After gaining control over the final architectures obtained from oligothiophene assembly, a major issue is then to organize them on a substrate following a predetermined scheme. In order for the nanostructures, which are generated in a controlled way, to be incorporated in plastic electronic devices, they have to be organized over large areas. Deposition of oligothiophene-based monolayers on contact electrodes made of conducting polymer layers (like PEDOT) is also possible. With the fundamental understanding of nanostructure building, mainly driven by self-assembling processes, making significant advances, the control of their organization on a surface constitutes the next step. Some attempts to use spatial deposition or soft-lithography-derived techniques have already shown very promising results[61−63] and will certainly be a determining approach soon, probably in combination with scanning probe microscopy-derived techniques. They can provide control of the organization of the nanostructures following predefined architectures as well as the characterization of the electrical properties on the local scale.

Acknowledgment. The collaboration between Mons, Eindhoven, Bologna, and Durham has been conducted within the European Commission Training and Mobility of Researchers Network LAMINATE (Large Area Molecular electronics Involving a Novel Approach to Training and Education, Contract Number HPRN-CT-2000-00135). The authors thank L. Brunsveld and M. Fransen for providing the penta(ethylene glycol)s. Research in Mons has been conducted within the framework of the Belgian Science Policy Interuniversity Attraction Poles Program (PAI V/3) and the European Science Foundation "Structuring, Manipulation, Analysis and Reactive Transformation of Nanostructures (SMARTON)" program. Research in Mons is also supported by the European Commission, the Government of the Région Wallonne (Phasing Out—Hainaut) and the Belgian National Fund for Scientific Research FNRS/FRFC. M.S. acknowledges the F.R.I.A. (Belgium) for a doctoral scholarship. Financial support from the Engineering and Physical Sciences Research Council and the University of Durham for, *interalia*, infrastructure, spectroscopic and analytical facilities is gratefully acknowledged.

References

(1) (a) Sariciftci, N. S.; Smilowitz, L.; Heeger, A. J.; Wudl, F. *Science* **1992**, *258*, 1474. (b) Yu, G.; Gao, J.; Hummelen, J. C.; Wudl, F.; Heeger, A. J. *Science* **1995**, *270*, 1789. (c) Halls, J. J. M.; Walsh, C. A.; Greenham, N. C.; Marseglia, E. A.; Friend, R. H. *Nature* **1995**, *376*, 498.

(2) Burroughes, J. H.; Bradley, D. D. C.; Brown, A. R.; Marks, R. N.; MacKay, K.; Friend, R. H.; Burn, P. L.; Holmes, A. B. *Nature* **1990**, *347*, 539.

(3) (a) Garnier, F.; Hajlaoui, R.; Yassar, A.; Srivastava, P. *Science* **1994**, *265*, 1684. (b) Lin, Y.-Y.; Gundlach, D. J.; Nelson, S. F.; Jackson, T. N. *IEEE Trans. Electron. Devices* **1997**, *44*, 1325.

(4) (a) Brown, A. R.; Pomp, A.; Hart, C. M.; de Leeuw, D. M. *Science* **1995**, *270*, 972. (b) Sirringhaus, H.; Tessler, N.; Friend, R. H. *Science* **1998**, *280*, 1741.

(5) (a) *Electronic Materials: The Oligomer Approach*; Müllen, K., Wegner, G., Eds.; VCH: Weinheim, 1998 (b) Horowitz, G. *Adv. Mater.* **1998**, *10*, 365. (c) Lovinger, A. J.; Katz, H. E.; Dodabalapur, A. *Chem. Mater.* **1998**, *10*, 3275. (d) Martin, R. E.; Diederich, F. *Angew. Chem., Int. Ed.* **1999**, *38*, 1350. (e) Dimitrakopoulos, C. D.; Malenfant, P. R. L. *Adv. Mater.* **2002**, *14*, 99.

(6) Tour, J. M. *Chem. Rev.* **1996**, *96*, 537.

(7) Fichou, D. *J. Mater. Chem.* **2000**, *10*, 571.

(8) Roncali, J. *Acc. Chem. Res.* **2000**, *33*, 147.

(9) See, for example: *Handbook of Oligo- and Polythiophenes*; Fichou, D., Ed.; Wiley-VCH: New York, 1999. Katz, H. E.; Bao, Z. *J. Phys. Chem. B* **2000**, *104*, 671.

(10) (a) McCullough, R. D. *Adv. Mater.* **1998**, *10*, 93. (b) Elsenbaumer, R. L.; Jen, K.-Y.; Oboodi, R. *Synth. Met.* **1986**, *15*, 169.

(11) (a) McCullough, R. D.; Löwe, R. D.; Jayaraman, M.; Ewbank, P. C.; Anderson, D. L.; Tristran-Nagle, S. *Synth. Met.* **1993**, *55*, 1198. (b) McCullough, R. D.; Löwe, R. D.; Jayaraman, M.; Anderson, D. L. *J. Org. Chem.* **1993**, *58*, 904. (c) Chen, T.-A.; Rieke, R. D. *J. Am. Chem. Soc.* **1992**, *114*, 10087.

(12) Katz, H. E.; Bao, Z.; Gilat, S. *Acc. Chem. Res.* **2001**, *34*, 359.

(13) (a) Katz, H. E. *J. Mater. Chem.* 1997, *7,* 369. (b) Yassar, A.; Horowitz, G.; Valat, P.; Wintgens, V.; Hmyene, M.; Deloffre, F.; Srivastava, P.; Lang, P.; Garnier, F. *J. Phys. Chem.* **1995**, *99*, 9155.

(14) Mazzeo, M.; Vitale, V.; Della Sala, F.; Pisignano, D.; Anni, M.; Barbarella, G.; Favaretto, L.; Zanelli, A.; Cingolani, R.; Gigli, G. *Adv. Mater.* **2003**, *15*, 2060.

(15) Ponomarenko, S. A.; Kirchmeyer, S.; Elschner, A.; Huisman, B.-H.; Karbach, A.; Drechsler, D. *Adv. Funct. Mater.* **2003**, *13*, 591.

(16) (a) Gellman, S. H. *Acc. Chem. Res.* **1998**, *31*, 173. (b) Seebach, D.; Matthew, J. L. *Chem. Commun.* **1997**, 2015. (c) Nelson, J. C.; Saven, J. G.; Moore, J. S.; Wolynes, P. G. *Science* **1997**, *277*, 1793. (d) Lokey, R. S.; Iverson, B. L. *Nature* **1995**, *375*, 303.

(17) Meskers, S. C. J.; Peeters, E.; Langeveld-Voss, B. M. W.; Janssen, R. A. J. *Adv. Mater.* **2000**, *12*, 589.

(18) (a) Gesquière, A.; Abdel-Mottaleb, M. M. S.; De Feyter, S.; De Schryver, F. C.; Schoonbeek, F. S.; van Esch, J. H.; Kellog, R. M.; Feringa, B. L.; Calderone, A.; Lazzaroni, R.; Brédas, J. L. *Langmuir* **2000**, *16*, 10385. (b) Rep, D. B. A.; Roelfsema, R.; van Esch, J. H.; Schoonbeek, F. S.; Kellog, R. M.; Feringa, B. L.; Palstra, T. T. M.; Klapwijk, T. M. *Adv. Mater.* **2000**, *12*, 563. (c) Schoonbeek, F. S.; van Esch, Wegewijs, B.; Rep, D. B. A.; de Haas, M. P.; Klapwijk, T. M.; Kellog, R. M.; Feringa, B. L. *Angew. Chem., Int. Ed.* **1999**, *38*, 1393.

(19) (a) Decher, G.; Schlenoff, J. B. in *Multilayer Thin Films* Wiley: Weinheim, 2003. (b) Decher, G. *Science* **1997**, *277*, 1232.

(20) (a) Zhai, L.; McCullough, R. D. *Adv. Mater.* **2002**, *14*, 901. (b) Locklin, J.; Youk, J. H.; Xia, C.; Park, M.-K.; Fan, X.; Advincula, R. C. *Langmuir* **2002**, *18*, 877. (c) Hassenkam, T.; Greve, D. R.; Bjørnholm, T. *Adv. Mater.* **2001**, *13*, 631. (d) Reitzel, N.; Greve, D. R.; Kjaer, K.; Howes, P. B.; Jayaraman, M.; Savoy, S.; McCullough, R. D.; McDevitt, J. T.; Bjørnholm, T. *J. Am. Chem. Soc.* **2000**, *122*, 5788. (e) Nakahara, H.; Nakayama, J.; Hoshino, M.; Fukuda, K. *Thin Solid Films* **1988**, *160*, 87. (f) Isz, S.; Weissbuch, I.; Kjaer, K.; Bouwman, W. G.; Als-Nielsen, J.; Palacin, S.; Ruaudel-Teixier, A.; Leiserowitz, L.; Lahav, M.

Chem. Eur. J. **1997**, *3*, 930. (g) Dutta, A. K.; Pal, A. J.; Misra, T. N. *Bull. Chem. Soc. Jpn.* **1993**, *66*, 3576.
(21) For a review on the self-assembly of conjugated polymers and oligomers, see: Berlin, A.; Zotti, G. *Macromol. Rapid Commun.* **2000**, *21*, 301.
(22) (a) Kilbinger, A. F. M.; Feast, W. J. *J. Mater. Chem.* **2000**, *10*, 1777. (b) Urban, V.; Wang, H. H.; Thiyagarajan, P.; Littrell, K. C.; Wang, H. B.; Yu, L. *J. Appl. Crystallogr.* **2000**, *33*, 645. (c) Ohsedo, Y.; Imae, I.; Shirata, Y. *Synth. Met.* **1999**, *102*, 969. (d) Hempenius, M. A.; Langeveld-Voss, B. M. W.; van Haare, J. A. E. H.; Janssen, R. A. J.; Sheiko, S. S.; Spatz, J. P.; Möller, M.; Meijer, E. W. *J. Am. Chem. Soc.* **1998**, *120*, 2798. (e) Donat-Bouillud, A.; Mazerolle, L.; Gagnon, P.; Goldenberg, L.; Petty, M. C.; Leclerc, M. *Chem. Mater.* **1997**, *9*, 2815. (f) Wei, Y.; Yang, Y.; Yeh, J.-M. *Chem. Mater.* **1996**, *8*, 2659. (g) Rutherford, D. R.; Stille, J. K.; Elliot, C. M.; Reichert, V. R. *Macromolecules* **1992**, *25*, 2294. (h) Henze, O.; Feast, W. J. *J. Mater. Chem.* **2003**, *13*, 1274.
(23) (a) Aratani, N.; Osuka, A.; Kim, Y. H.; Jeong, D. H.; Kim, D. *Angew. Chem., Int. Ed.* **2000**, *39*, 1458. (b) Davies, W. B.; Svec, W. A.; Ratner, M. A.; Wasielewski, M. R. *Nature* **1998**, *396*, 60.
(24) Moore, J. S.; Zhang, J. *Angew. Chem., Int. Ed. Engl.* **1992**, *31*, 922.
(25) (a) Kolb, D. M.; Engelmann, G. E. *Angew. Chem., Int. Ed.* **2000**, *39*, 922. (b) Engelkamp, H.; Middelbeek, S.; Nolte, R. M. J. *Science* **1999**, *284*, 785.
(26) (a) Hotta, S.; Waragai, K. *Adv. Mater.* **1993**, *5*, 896. (b) Sirringhaus, H.; Brown, P. J.; Friend, R. H.; Nielsen, M. N., Bechgaard, K.; Langeveld-Voss, B. M. W.; Spiering, A. J. H.; Janssen, R. A. J.; Meijer, E. W.; Herwig, P.; De Leeuw, D. M. *Nature* **1999**, *401*, 685. (c) Horowitz, G.; Hajlaoui, M. E. *Adv. Mater.* **2000**, *12*, 1046.
(27) Henze, O.; Parker, D.; Feast, W. J. *J. Mater. Chem.* **2003**, *13*, 1269.
(28) (a) Kilbinger, A. F. M.; Schenning, A. P. H. J.; Goldoni, F.; Feast, W. J.; Meijer, E. W. *J. Am. Chem. Soc.* **2000**, *122*, 1820. (b) Schenning, A. P. H. J.; Kilbinger, A. F. M.; Biscarini, F.; Cavallini, M.; Cooper, H. J.; Derrick, P. J.; Feast, W. J.; Lazzaroni, R.; Leclère, P.; McDonnel, L. A.; Meijer, E. W.; Meskers, S. C. J. *J. Am. Chem. Soc.* **2002**, *124*, 1269.
(29) (a) Katz, H. E.; Dodabalapur, A.; Torsi, L.; Elder, D. *Chem. Mater.* 1995, *7*, 2238. (b) Parakka, J. P.; Cava, M. P. *Tetrahedron* **1995**, *51*, 2229. (c) Katz, H. E. *J. Mater. Chem.* 1997, *7*, 369. (d) Katz, H. E.; Laquindanum, J. G.; Lovinger, A. J. *Chem. Mater.* **1998**, *10*, 633.
(30) See for a solid-state spectrum of α-6T: Muccini, M.; Lunedei, E.; Taliani, C.; Beljonne, D.; Cornil, J.; Brédas, J. L. *J. Chem. Phys.* **1998**, *109*, 10513.
(31) Kilbinger, A. F. M.; Cooper, H. J., McDonnel, L. A.; Feast, W. J.; Derrick, P. J.; Schenning, A. P. H. J.; Meijer, E. W. *ChemComm.* **2000**, 383.
(32) See also: (a) Palmans, A. R. A.; Vekemans, J. A. J. M.; Havinga, E. E.; Meijer, E. W. *Angew. Chem., Int. Ed. Engl.* **1997**, *36*, 2648. (b) Sandström, J. *Circular Dichroism: Principles and Applications*; Nakanishi, K., Berova, N., Woodey, R., Eds.; VCH: Weinheim, 1994.
(33) Langeveld-Voss, B. M. W.; Beljonne, D.; Shuai, Z.; Janssen, R. A. J.; Meskers, S. C. J.; Meijer, E. W.; Brédas, J. L. *Adv. Mater.* **1998**, *10*, 1343.
(34) McRea, E. G.; Kasha, M. *J. Phys. Chem.* **1958**, *28*, 721.
(35) Further evidence of this temperature-dependent reversible aggregation of **3b** in deuterated *n*-butanol was obtained from the NMR spectra of 12 mM solution: broad lines were observed below 90 °C and sharp ones above.
(36) While melting is strictly concerned with the crystal to liquid state transition, we adopt the practice of the biological sciences in referring to the disruption of highly organized aggregates in fluid media as melting; see: Saenger W. *Principles of Nucleic Acid Structure*; Springer-Verlag: New York, 1984; p 143.
(37) Apperloo, J. J.; Janssen, R. A. J.; Malenfant, P. R. L.; Fréchet, J. M. J. *Macromolecules* **2000**, *33*, 7038.
(38) Brunsveld, L.; Zhang, H.; Glasbeek, M.; Vekemans, J. A. J. M.; Meijer E. W. *J. Am. Chem. Soc.* **2000**, *122*, 6175.
(39) Prince, R. B.; Brunsveld, L.; Meijer, E. W.; Moore, J. S. *Angew. Chem Int. Ed.* **2000**, *39,* 228.
(40) Kirschbaum, T.; Bauërle, P. *Synth. Met.* **2001**, *119*, 127.
(41) Green, M. M.; Reidy, M. P.; Johnson, R. D.; Darling, G.; O'Leary, D. J.; Wilson G. *J. Am. Chem. Soc.* **1989**, *111*, 6452.
(42) Brunsveld, L.; Schenning, A. P. H. J.; Broeren, M. A. C.; Janssen, H. M.; Vekemans, J. A. J. M.; Meijer, E. W. *Chem. Lett.* **2000**, 292.
(43) (a) Lifson, S.; Andreola, C.; Peterson, N. C.; Green, M. M. *J. Am. Chem. Soc.* **1989**, *111*, 8850. (b) Green, M. M.; Sato, T.; Teramoto, A.; Lifson, S. *Macromol. Symp.* **1996**, *101*, 363. (c) Langeveld-Voss, B. M. W.; Waterval, R. J. M.; Janssen, R. A. J.; Meijer, E. W. *Macromolecules* **1999**, *32*, 227.
(44) Ostoja, P.; Guerri, G.; Rossini, S.; Servidori, M.; Taliani, C.; Zamboni, R. *Synth. Met.* **1993**, *54*, 447.
(45) Servet, B.; Ries, S.; Trotel, M.; Alnot, P.; Horowitz, G.; Garnier, F. *Adv. Mater.* **1993**, *5,* 461.
(46) Lovinger, A. J.; Davis, D. D.; Ruel, R.; Torsi, L.; Dodabalapur, A.; Katz, H. E. *J. Mater. Res.* **1995**, *10*, 2958.
(47) Servet, B.; Horowitz, G.; Ries, S.; Lagorse, O.; Alnot, P.; Yassar, A.; Deloffre, F.; Srivastava, P.; Hajlaoui, R.; Lang, P.; Garnier, F. *Chem. Mater*. **1994**, *6*, 1089.
(48) Böhme, O.; Ziegler, Ch.; and Göpel, W. *Synth. Met*. **1994**, *67*, 87.
(49) Egelhaaf H.-J. and Oelkrug, D. *Proc. SPIE* **1995**, *2362*, 398.
(50) Oeter, D.; Egelhaaf, H.-J.; Ziegler, Ch.; Oelkrug, D.; Göpel, W. *J. Chem. Phys.* **1994**, *101*, 6344.
(51) Biscarini, F.; Zamboni, R.; Samorì, P.; Ostoja, P.; Taliani, C. *Phys. Rev. B*, **1995**, *52*, 14868.
(52) Biscarini, F.; Greco, O.; Lauria, A.; Zamboni, R.; Taliani, C. *Mol. Cryst. Liq. Cryst.* **1996**, *290*, 203.
(53) Viville, P.; Lazzaroni, R.; Brédas, J. L.; Moretti, P.; Samorí, P.; Biscarini, F. *Adv. Mater.* **1998**, *10*, 57.
(54) Biscarini, F. *In Scanning Probe Microscopy of Polymers*; Ratner, B., Tsukruk, V. V., Eds.; ACS: Washinghton DC, 1998.
(55) Barabási A.-L.; Stanley, H. E. In *Fractal Concepts in Surface Growth;* Cambridge University: Cambridge, UK, 1995.
(56) Egelhaaf, H.-J.; Bäuerle, P.; Rauer, K.; Hoffmann, V.; Oelkrug, D. *Synth. Met.* **1993**, *61*, 143.
(57) Molecular Mechanics simulations were performed using Cerius2 from Accelrys, using UFF as force field; see: (a) Rappé, A. K.; Casewit, C. J.; Colwell, K. S.; Goddard, W. A., III; Skiff, W. M. *J. Am. Chem. Soc.* **1992**, *114*, 10024. (b) Casewit, Colwell, K. S., Rappé, A. K. *J. Am. Chem. Soc.* **1992**, *114*, 10046). The nonbonded interactions are described using the Spline method, with spline-on and spline-off parameters set to 11 and 14 Å, respectively. Convergence is reached using the conjugate gradient with a rms force of 10^{-3} kcal/mol Å.
(58) Zhang, Y.; Lu, R.; Song, Y.; Jiang, L.; Liu, Y.; Zhao, Y.; Li, T. J. *Thin Solid Films* **2003**, *437*, 150.
(59) Leclère, Ph.; Surin, M.; Henze, O.; Jonkheijm, P.; Biscarini, F. Cavallini, M.; Feast, W. J.; Kilbinger, A. F. M.; Lazzaroni, R.; Meijer, E. W.; Schenning A. P. H. J. *J. Mater. Chem.* **2004**, *14*, 1959.
(60) (a) Sandberg, H.; Henze, O.; Sirringhaus, H.; Kilbinger, A. F. M.; Feast, W. J.; and Friend, R. H. *Proc. SPIE* **2001**, *4466*, 35. (b) Sandberg, H.; Henze, O.; Kilbinger, A. F. M.; Sirringhaus, H.; Feast, W. J.; Friend, R. H *Synth. Met.* **2003**, *137*, 885.
(61) Holdcroft, S. *Adv. Mater*. **2001**, *13*, 1753.
(62) (a) Xia, Y.; Whitesides, G. M. *Annu. Rev. Mater. Sci.* 1998, *28*, 153. (b) Xia, Y.; Rogers, J. A.; Paul K. E., Whitesides, G. M. *Chem. Rev.* 1999, *99*, 1823. (c) Behl, M.; Seekamp, J.; Zankovych, S.; Sotomayor Torres, C. M.; Zentel, R.; Ahopelto, J. *Adv. Mater.* **2002**, *14*, 588.
(63) (a) Cavallini, M.; Biscarini, F.; Massi M.; Farran-Morales, A.; Leigh, D. A.; Zerbetto, F. *Nanoletters* **2002**, *2*, 635; (b) Cavallini, M.; Biscarini, F. *Nanoletters* **2003**, *3*, 1269. (c) Pisignano, D.; Persano, L.; Cingolani, R.; Gigli G.; Babudri F.; Farinola G. M.; Naso F. *Appl. Phys. Lett.* **2004**, *84*, 1365.

CM049673X